

Article

Biomechanical Effects of Medializing Calcaneal Osteotomy on Bones and the Tissues Related to Adult-Acquired Flatfoot Deformity: A Computational Study

Javier Bayod ^{1,*}, Ricardo Larrainzar-Garijo ², Brayan David Solórzano ³ and Christian Cifuentes-De la Portilla ³ 

¹ Applied Mechanics and Bioengineering Group (AMB), Aragón Institute of Engineering Research (I3A), Universidad de Zaragoza, 50018 Zaragoza, Spain

² Orthopaedics and Trauma Department, Medicine School, Hospital Universitario Infanta Leonor, Universidad Complutense, 28031 Madrid, Spain

³ Biomedical Engineering Department, Universidad de los Andes, Bogotá 111711, Colombia

* Correspondence: jbayod@unizar.es

Abstract: Medializing calcaneal osteotomy (MCO) is a flatfoot treatment in stages IIa–IIb. It is true that structural correction is well known, but stress changes in foot tissues have not been sufficiently studied to date. Our objective was to evaluate the stress generated by MCO in both hindfoot and forefoot bones and in some soft tissues that support the arch. A finite element foot model was employed, simulating some situations related to flatfoot development. Results show a higher stress concentration around the osteotomy region when MCO is used in patients with plantar fascia weakness. Additionally, the stress increase found in lateral metatarsals would be the explanation for the long-term pain reported by patients.

Keywords: finite elements; flatfoot; stress redistribution; osteotomy; pes planus

MSC: 92-08



Citation: Bayod, J.; Larrainzar-Garijo, R.; Solórzano, B.D.; Cifuentes-De la Portilla, C. Biomechanical Effects of Medializing Calcaneal Osteotomy on Bones and the Tissues Related to Adult-Acquired Flatfoot Deformity: A Computational Study. *Mathematics* **2023**, *11*, 2243. <https://doi.org/10.3390/math11102243>

Academic Editors: Fernando Simoes and Mauro Malvè

Received: 22 February 2023

Revised: 19 April 2023

Accepted: 29 April 2023

Published: 10 May 2023



Copyright: © 2023 by the authors. Licensee MDPI, Basel, Switzerland. This article is an open access article distributed under the terms and conditions of the Creative Commons Attribution (CC BY) license (<https://creativecommons.org/licenses/by/4.0/>).

1. Introduction

Adult acquired flatfoot deformity (AAFD) is a pathology that causes a progressive flattening of the foot arch, which has been traditionally related to a tibialis posterior tendon (TPT) dysfunction. However, some clinical studies found that a failure/rupture of the plantar fascia (PF) or the calcaneonavicular ligament (also spring ligament (SL)) could also generate the arch collapse and the forefoot abduction [1–5]. Treatment options depend on the injury stage. In the first stages, AAFD treatments are related to reinforcing the TPT [6]. Nevertheless, sometimes the foot deformation reappears over time, forcing surgeons to use more aggressive techniques, intervening directly over the foot's bone structure. If the foot deformity is still flexible (stages IIa and IIb), the most habitual procedure is medializing calcaneal osteotomy (MCO) [7,8], which allows both the progressive foot arch flattening and the foot pronation caused by the flatfoot deformity to be corrected [4,6,9]. This procedure provokes a supination momentum in the foot to compensate the pronation [1,10]. In this way, the foot's structural correction is achieved by MCO and its results are normally satisfactory. Nevertheless, some clinical studies have shown that this procedure generates long-term side-effects related to stress distribution changes in forefoot and metatarsals [11–13], which could increase the risk of bone fractures, as has been reported with Evans' osteotomy [14].

In a recent study published by our research group using a previous version of our foot model, we showed that MCO can reduce foot pronation on its own [9]. However, changes in the biomechanical stress caused in bones and the main soft tissues that support the arch remained unstudied. Even in the literature, these stress changes have not been sufficiently studied, because of the difficulty of measuring tissue stresses in cadavers.

Some cadaver-based models have been used to study the structural correction of the foot, evaluating changes in both the plantar footprint using force platforms, and foot arch falling using radiographic (Rx) images. For example, Patrick et al. [15] measured the subtalar joint pressure produced by MCO using a cadaveric model suffering with flatfoot. They introduced a pressure sensor in the posterior facet joint, obtaining some, but limited, information about the effects of MCO on hindfoot joint pressures. As can be noted, these kinds of studies require high economic investment in measurement equipment, as well as meticulous control over the tested tissues to guarantee their biomechanical characteristics [16].

An alternative now accepted by clinicians and biomechanical researchers for evaluating the complex biomechanics of the human foot is finite element modelling (FEM) [17–19]. There are many models that study foot biomechanics and the effects produced by some surgical techniques. However, none of them have been used to study the stress effects of MCO on foot tissues. This kind of model specifically evaluates foot structure deformation and plantar pressure measurement [13,19]. Thus, these models greatly simplify the tissue anatomy and do not take into account important aspects such as the biomechanical difference between cortical and trabecular bones (which is very important when tissue stresses are evaluated [20], nor the geometry of some soft tissues such as the plantar fascia, the spring ligament, ligaments, or tendons, which are habitually modelled as bar elements. Thus, previously reported models cannot measure and locate the stresses around the foot anatomy.

The objective of this research was to investigate the biomechanical effects in terms of stress concentrations and displacements that an MCO provokes in both foot bones and the main foot arch stabilizers (TPT, PF and SL), using an enhanced version of the model used in [9]. This analysis was performed by simulating different pathological scenarios related to AAFD development.

2. Materials and Methods

This study was based on the foot model (segmentation and tissue properties) proposed by Cifuentes-De la Portilla et al [3], which has been used for the flatfoot evaluation of some other surgical procedures [21]. However, for this study, the entire model was reconstructed to simulate the MCO procedure, maintaining both tissue characteristics and loading conditions but including both the tibia and fibula bones to better represent the anatomical tendons' trajectories. The model used reconstructed a healthy human unloaded foot, based on CT images (radiographs of 0.6 mm/slide) acquired from the right foot of a 49-year-old man (weight = 75 Kg, height = 1.70 m).

2.1. FE Foot Model and Modifications

Tissue segmentation and 3D reconstruction (bones, PF, TPT, Achilles' tendon, Peroneus Longus tendon (PLT) and Peroneus Brevis tendon (PBT)) were performed using MIMICS V. 10 (Materialize, Leuven, Belgium). The spring ligament (SL) and both plantar ligaments (short plantar ligament and long plantar ligament) were added following atlas images, following the surgeons' guidance due to the difficulty of segmenting these from the CT images. The tibia and fibula were reoriented with tools available in MIMICS from the scan position to correspond to the orientation during the stance phase of gait. The previous finite element model [9] was enhanced by adding the TPT, Achilles' tendon, PLT, and PBT.

To simulate the MCO, calcaneus bone was modified, performing a 45-degree transversal cut and translating the segment medially by 10-mm (See Figure 1) [15,22]. This modification was performed following the guidance of a specialist in foot surgeries. Elements allowing internal fixation, such as plates, screws, and bone graft, were not simulated because a complete joint fusion was supposed. The complete FE model is shown in Figure 1.

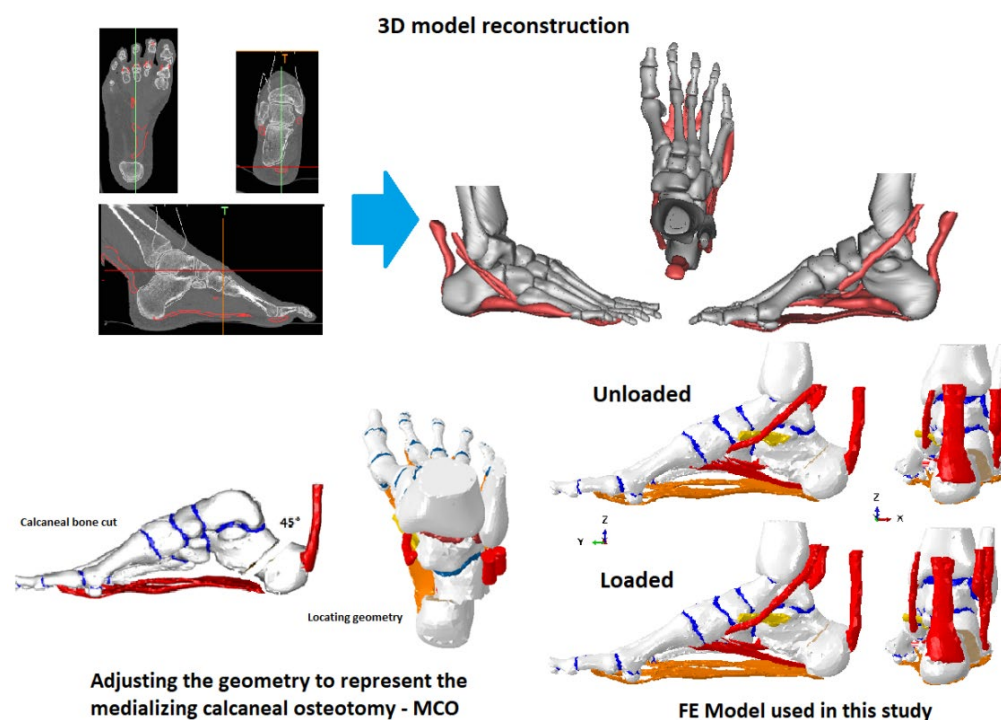


Figure 1. Reconstruction and modifications in the model to simulate a medializing calcaneal osteotomy. The Achilles’ tendon, tibialis posterior tendon, and both Peroneus tendons’ geometries and the pieces of Tibia and Fibula bones were reoriented to obtain a vertical position.

2.2. Meshing

The model’s meshing was developed by means of the software ANSYS V.15 (Canonsburg, PA, USA). In summary, the model include 28 cortical bone pieces, 24 trabecular bone pieces, 26 cartilage segments, 4 tendons, 3 ligaments, and the plantar fascia. A trial–error approach was used to optimize the mesh size of each segment [17]. These authors suggested that the number of inaccurate elements must be less than 5% in all the measured parameters. All simulations and post-processing were developed in Abaqus/CAE 6.14 (Dassault Systèmes, Vélizy-Villacoublay, France) using the available nonlinear geometry solver.

Some of the conditions considered in order to achieve a reasonable mesh size without compromising the calculation time included having a minimum mesh size sufficiently small to fit into the tightest segments, a mesh accuracy of more than 99% of the elements being better than 0.2 mesh quality (Jacobians) and checking that the poor elements were located away from the region of greatest interest (hindfoot bones, metatarsals, PF, and SL) (see Figure 2). The convergence analysis was performed for 265,547 linear tetrahedral elements (C3D4). All parameters exhibited good mesh quality ratios (see Table 1).

Table 1. Mesh quality metrics based on Burkhart et al. (2013) recommendations [17].

Quality Metric	Assessment Criteria	Accurate Elements	Inaccurate Elements
Element Jacobians	>0.2	99.96%	0.04%
Aspect ratio	>0.3	96.9%	3.1%
Min. angles	>30°	95.3%	4.7%
Max. angles	<120°	99.46%	0.84%

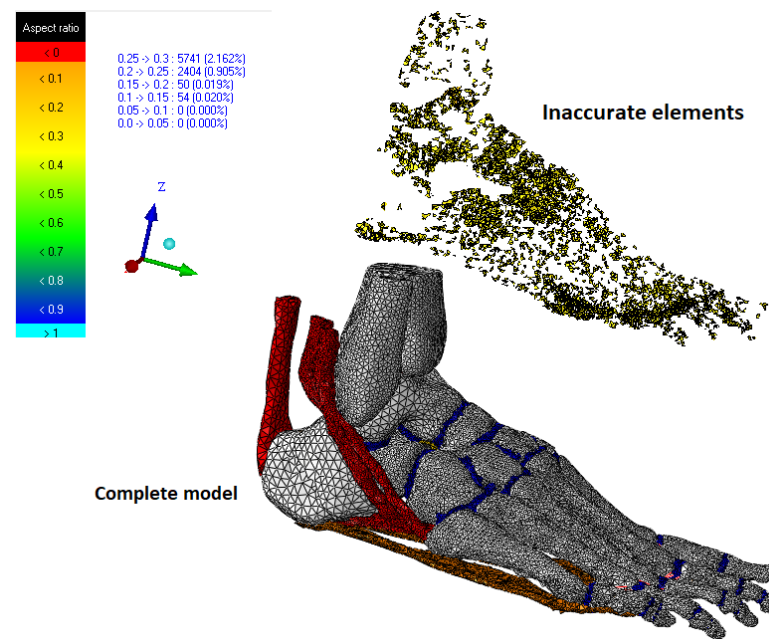


Figure 2. Location of the inaccurate elements, applying the Jacobians as the quality mesh criteria for evaluation.

2.3. Tissue Properties

Two kinds of behavior were considered in this finite element model: linear elastic behavior and hyper-elastic behavior.

Tissues with elastic linear behavior were the cortical bone, trabecular bone, ligaments, and plantar fascia.

Tissues with hyper-elastic behavior were tendons and cartilages.

The numerical values for each of these tissues were as follows:

The material properties (Young’s modulus (E) and Poisson’s ratio (ν)) of the cortical bone, trabecular bone, ligaments, and plantar fascia were assigned in accordance with published data: cortical bone ($E = 17,000$ MPa, $\nu = 0.3$), trabecular bone ($E = 700$ MPa, $\nu = 0.3$), ligaments ($E = 250$ MPa, $\nu = 0.28$), and plantar fascia ($E = 240$ MPa, $\nu = 0.28$) [16,20,23].

Tendons and cartilages were modelled as hyper-elastic materials (Ogden model), using the parameters taken from specialized articles [24]. The strain energy density function U is:

$$U = \frac{\mu}{\alpha^2} (\lambda_1^\alpha + \lambda_2^\alpha + \lambda_3^\alpha - 3) + \frac{1}{D} (J - 1)^2, \tag{1}$$

where the initial shear modulus $\mu = 4.4$ MPa (cartilage)/33.16 MPa (tendons), the strain hardening exponent $\alpha = 2$ (cartilage)/24.89 (tendons), and the compressibility parameter $D = 0.45$ (cartilage)/0.0001207 (tendons) [16,24,25]. The plantar fascia and spring ligament failures were simulated, applying the isotropic hardening theory that generates a progressive reduction of the tissue’s stiffness, resulting in a very flexible material. The initial parameters were a Young’s modulus of 240 and a Poisson ratio of 0.3. This strategy allowed us to improve the convergence of the model. Tibialis posterior tendon failure was simulated by removing the traction force of this tendon. Additionally, we considered that this characterization could be more realistic than simply changing the properties of the tissues because it approximates the viscoelastic behavior of these tissues, where stiffness depends on the loading application. The model used for this study maintains the differences of the bone characterization (cortical and trabecular) presented in Cifuentes-De la Portilla, C. et al. [3], where the internal parts of all the foot bones were modeled as trabecular. However, fibula and tibia bones were entirely simulated as cortical because a stress evaluation was not performed on these parts.

2.4. Loading and Boundary Conditions

The FE model was reconstructed from CT images of an unloaded foot. First of all, a standing load position was created (midstance phase) that was used as a reference case to compare against all the pathological cases. In Figure 3, load and boundary conditions are shown. The value of 720 N for the load corresponds to the full weight of an adult of about 70 Kg leaning on one foot. This condition represents a traditional scenario of an AAFD diagnosis assessment. Both loading conditions and boundaries were kept unaltered for all the MCO simulations.

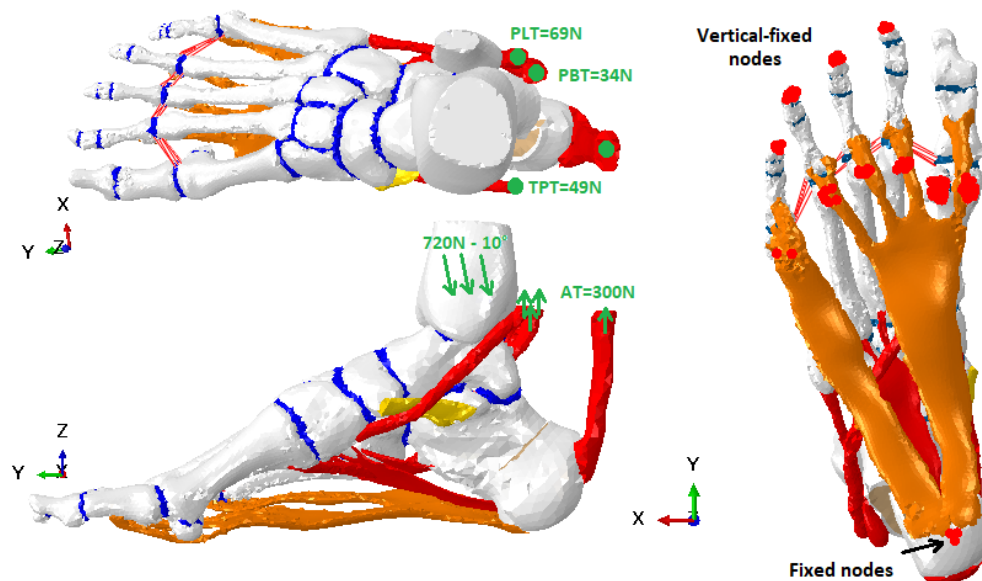


Figure 3. Boundary and loading values applied in the model. Loading values correspond to the weight of a person of 70 Kg.

The direction of the load exhibits an inclination of 10 degrees (descending vertical). This load was distributed over the tibia–talus joint (90%) and fibula–talus (10%) [26]. The tendon traction forces were included as reported by Arangio et al. [27]. To simulate the contact with the floor and to avoid the foot structure displacement under loading tests, some nodes located at the lower part of the calcaneus were fixed, while the Z-axis displacement (vertical) of the lower nodes of the first and fifth metatarsals was constrained to 0, using boundary tools available in Abaqus. The nodes remained unaltered for all the simulations performed. To avoid the tendon geometries crossing through the bones, we used the contact surfaces method, using the surfaces of the bones and tendons in contact during simulations.

2.5. About the Model Validation

This study used a model that has been previously validated for other studies related to AAFD [9]. They followed the recommendations of Tao et al. [5], measuring the vertical displacements of some anatomical points: the highest point of the talus (TAL) and of the navicular (NAV), the midpoint of the first cuneiform (CUN), and the highest point of the first metatarsal head (1MT), in two different loading conditions: light loading (minimal contact with the ground) and normal stance loading, using lateral Rx images (sagittal plane) (see Figure 4). The light loading condition was the position before starting simulations.

2.6. Model Analysis and Evaluation Criteria

To quantify the structural deformation of the foot and to evaluate biomechanical stress changes generated by MCO in foot tissues, we simulated the weakness/failure of the plantar fascia (PF), spring ligament (SL) and the tibialis posterior tendon (TPT) in isolation, but also combining these three elements. The weakness/failure was simulated by applying the isotropic hardening theory. This method was implemented using the function

“Parameter” in Abaqus, which allows modification of the stiffness of a material, reducing the Young’s modulus from its initial value until obtaining a stiffness reduction by about 86%. The stresses in hindfoot bones, forefoot bones, and in all the soft tissues included in the model were calculated.

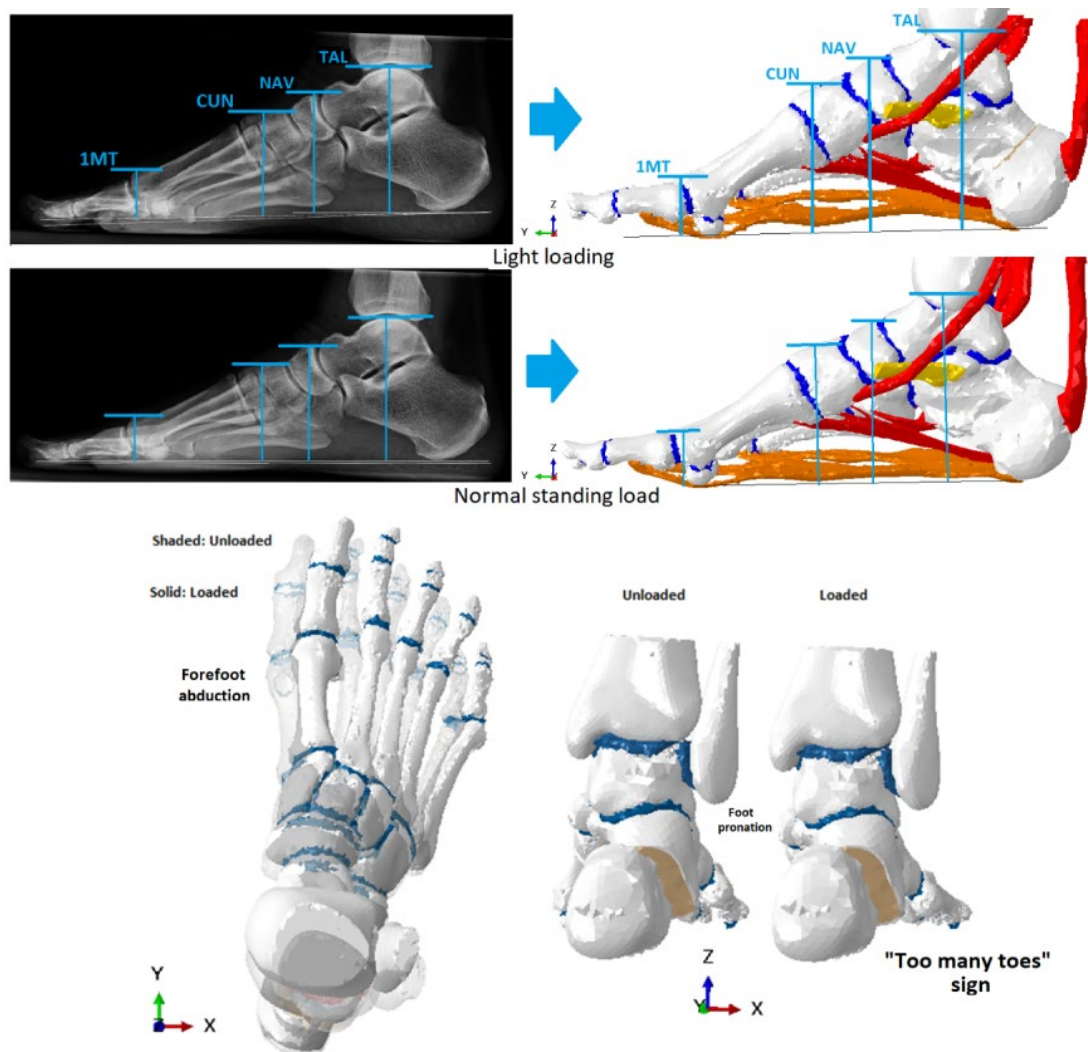


Figure 4. (Up) Validation strategy which compares the foot deformation in two different loading values. (Bottom) Signs of adult acquired flatfoot deformity achieved with our model.

For measuring stress on tissues, the maximum principal stress (S. Max) was used. This magnitude is closely related to the tensile stress that is generated in foot tissues [28]. Structural deformation was quantified measuring the vertical displacement of the entire structure (in millimeters).

3. Results

3.1. About Model Validation

Deformation found in the model is very approximated for a patient in a loading test. Found values can be included in the inter-subject variability under healthy conditions, represented as light loading (minimal contact with the ground) and a normal standing load (Table 2). These were compared with the average deformation of all the evaluated points measured in Rx-images in the sagittal view of 12 healthy patients.

Table 2. Results of the validation process. The values correspond to the difference between the measured distance from each point to the ground, under two different loading values: Light loading (minimal contact with the ground) and normal standing load [9].

Reference Point	Model Prediction (mm)	Patient Average (mm)	Patient Std. Deviation
TAL	−0.33	−0.32	0.14
NAV	−0.27	−0.26	0.04
CUN	−0.26	−0.19	0.08
1MT	−0.07	0.08	0.003

3.2. Flatfoot Simulation and MCO Structural Correction

Quantification of structural changes generated by both the simulated pathological scenarios and the MCO cases was carried out by measuring the vertical displacement of the entire foot skeletal structure (in millimeters). The values show by how much each foot region falls or rises (see Figure 5). Blue represents falling while red represents elevation. As can be seen, in simulations performed before applying MCO, the medial foot region suffers higher displacements downwards. These changes are also related to arch lengthening and foot pronation. After applying MCO, the tendency towards supination of the foot structure can be seen clearly, also causing fewer vertical displacements and less arch lengthening because of this (please see the Hallux fingertip—the tip of the big toe).

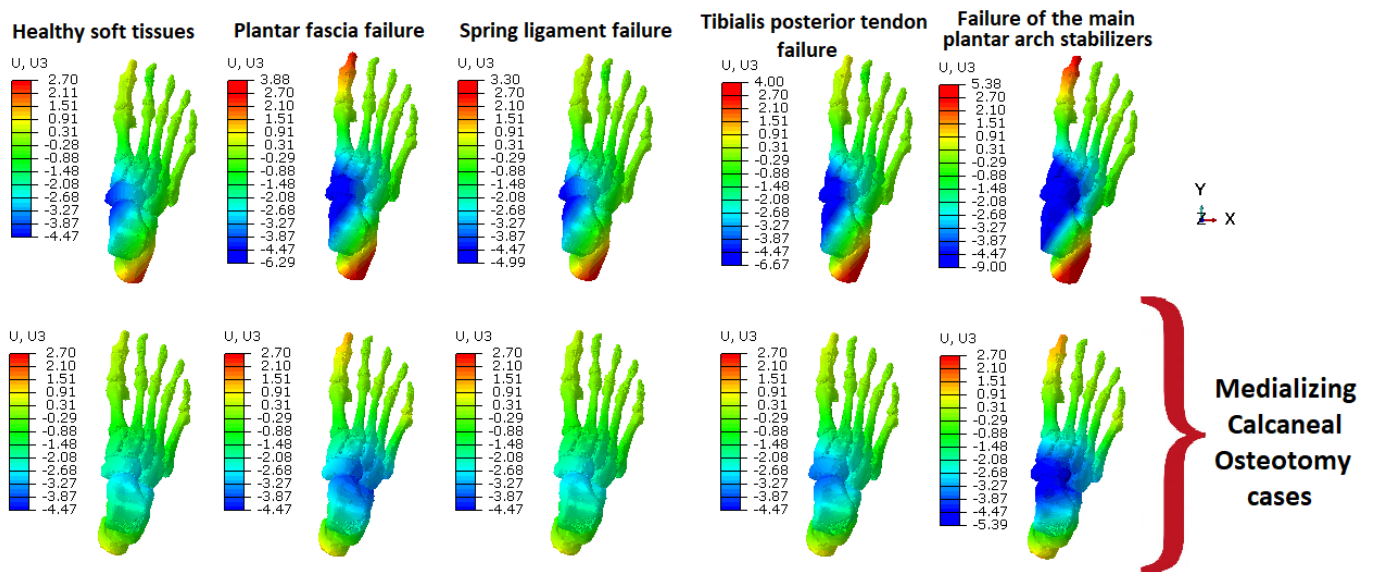


Figure 5. Structural changes obtained after simulating the model in different pathological cases. Values measure vertical displacement. Blue represents negative displacement (downwards). The color scale was normalized to 2.70, which is the maximum displacement reported in the healthy case. The maximum displacement values when these are higher than the reference is shown at the top of the color scale.

The effectiveness of MCO in the correction of the forefoot pronation and hindfoot valgus can be seen. Additionally, it can be observed how well MCO can compensate for the failure of both the spring ligament and the tibialis posterior tendon, reducing the effects expected by these failures (mainly forefoot pronation) [3,9].

The medialization of the calcaneus, through an osteotomy, manages to reduce the typical pronator moment of the subtalar joint. In this situation, the functional demand of the native structures to preserve the plantar arch, spring ligament, and tibiabis posterioris is significantly lower. If the pronator moment is maintained, the mechanical

demands are very high and this may explain the known failure in isolated arthrodeses of the talocuneiform joint.

3.3. Stress in Forefoot Bones Generated by MCO

The first analyzed results were stresses on metatarsals. This magnitude was measured in Megapascals (MPa). The color scale was normalized to 60 MPa to better visualize the results (Figure 6). However, for each color scale, we also show the highest value obtained from each case and the stress measured in lateral metatarsals. Meaning of the scale: red means high stress, green represents medium stress, while blue represents low stress. It is observed that MCO increases the stress around the fourth metatarsal, and it increases even more when the PF or TPT fails. Additionally, the MCO reduces the forefoot maximum stress by approximately 35% (from 240,04 MPa to 155,06 MPa). These results are relevant because they show how the MCO by itself caused this stress reduction in metatarsals.

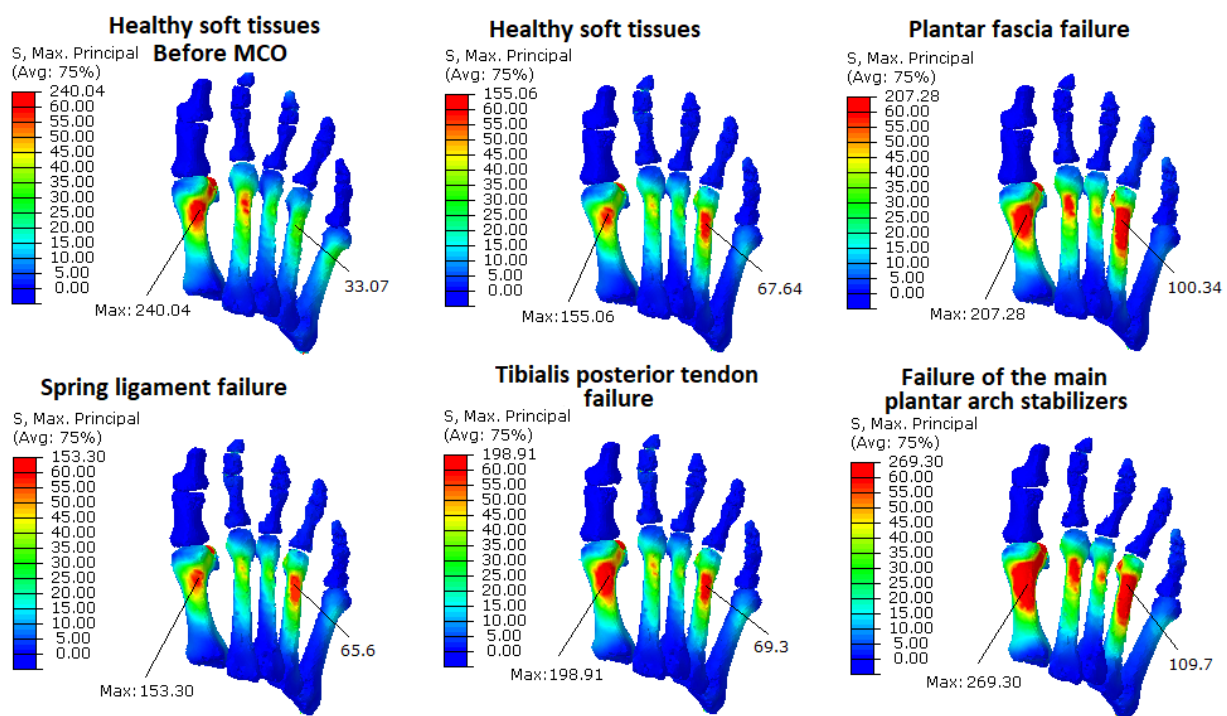


Figure 6. Stress in metatarsals (MPa). All simulations were performed after applying MCO, except for the first case which was included for comparison. The maximum stress values obtained are shown at the top of the color scale.

3.4. Stress in Hindfoot Bones Generated by MCO

In the second place, stresses in hindfoot bones were also evaluated for all the above-mentioned pathological cases for MCO (Figure 7). Now, the color scale for stress values was normalized to 20 MPa to better visualize the results. It can be noted that there is an increase in the stress concentration around the osteotomized region, when one of the main stabilizers fails (PF, TPT or SL).

A summary of bones stress changes is shown in Table 3, including the relative changes obtained from each case against simulating an MCO with healthy soft tissues. The results in Table 3 come from the stress results shown in Figures 6 and 7.

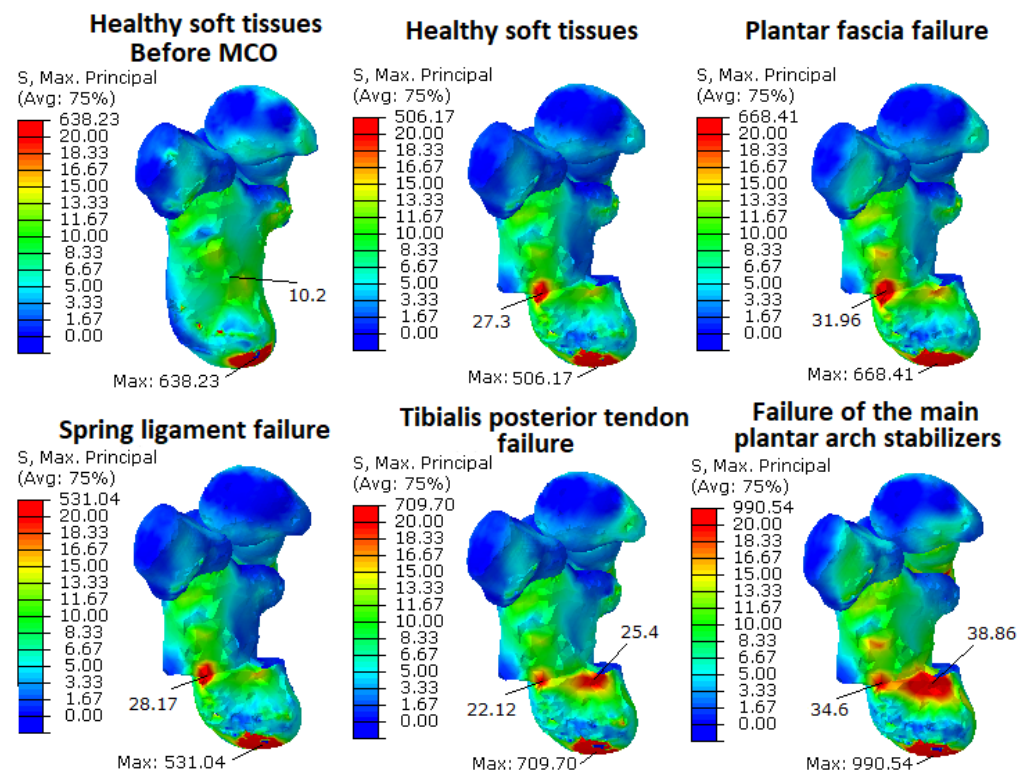


Figure 7. Stress in hindfoot bones (MPa). All simulations were performed after applying MCO, except for the first case which was included for comparison. The maximum stress values obtained are shown at the top of the color scale.

Table 3. Relative differences obtained from simulations, considering the simulation of MCO with healthy soft tissues as reference. This table is related to Figures 6 and 7. Please see these figures to find the maximum stress locations. All stress values are in megapascals (MPa).

	Forefoot Bones Stress		Hindfoot Bones Stress	
	Max. Stress Values (MPa)	Relative Difference (%)	Max. Stress Values (MPa)	Relative Difference (%)
Healthy after MCO	155.06	0	507.17	0
MCO and PF failure	207.28	34	668.41	32
MCO and SL failure	153.3	−1	531.04	5
MCO and TPT failure	198.91	28	709.7	40
MCO and main arch-stabilizers failure	269.3	74	990.54	95

3.5. Stress in Soft Tissues after MCO

We compared the soft tissue stress before and after applying MCO, simulating a failure of one or two of the main stabilizers of the plantar arch (TPT, PF and SL) (Figure 8). The results were normalized using values that allow the differences to be easily identified: 100 MPa for the tibialis posterior tendon, 33 MPa for the plantar fascia and 29 MPa for the spring ligament. The color scale is organized in the same way as described above for the bone stress evaluation.

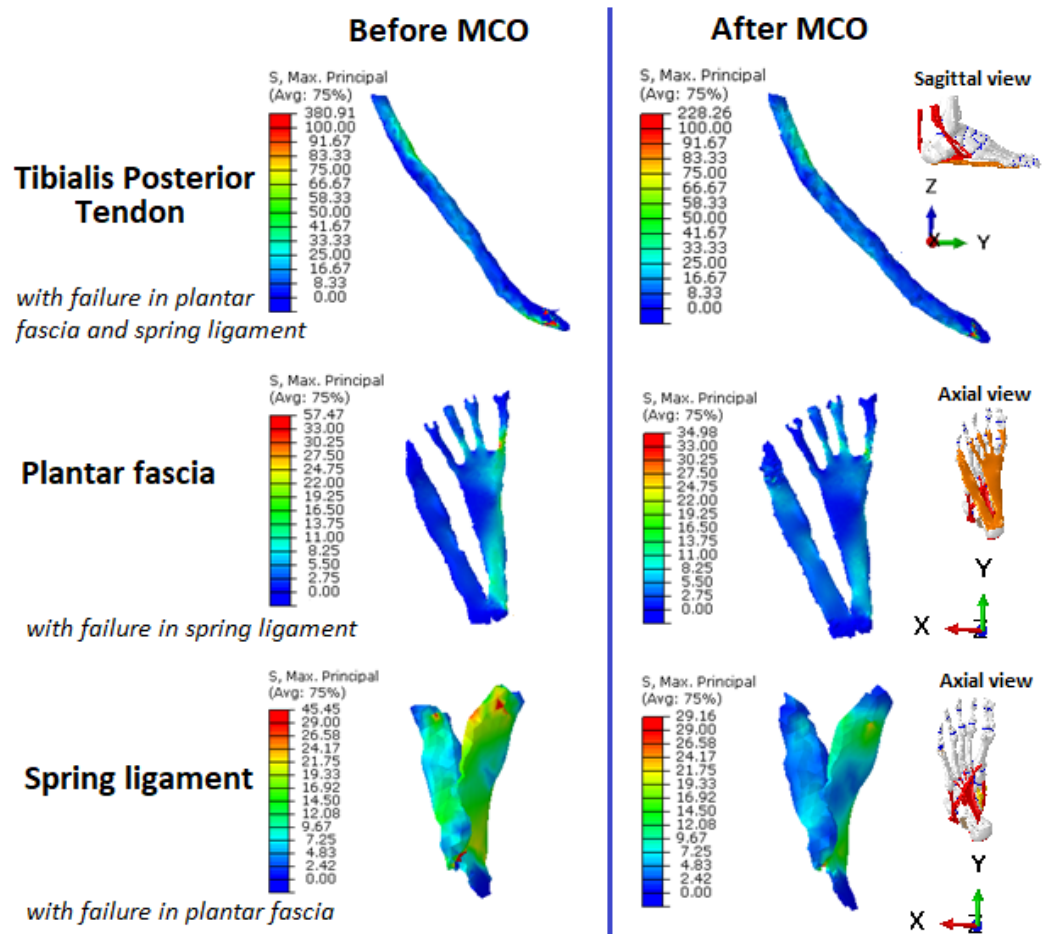


Figure 8. Comparison between stresses generated before and after applying MCO in the main soft tissues that support the plantar arch, in some pathological scenarios. The maximum stress values (MPa) obtained are shown at the top of the color scale.

The maximum stresses in the rest of the soft tissues included in the model were also quantified. The results are summarized in Figure 9.

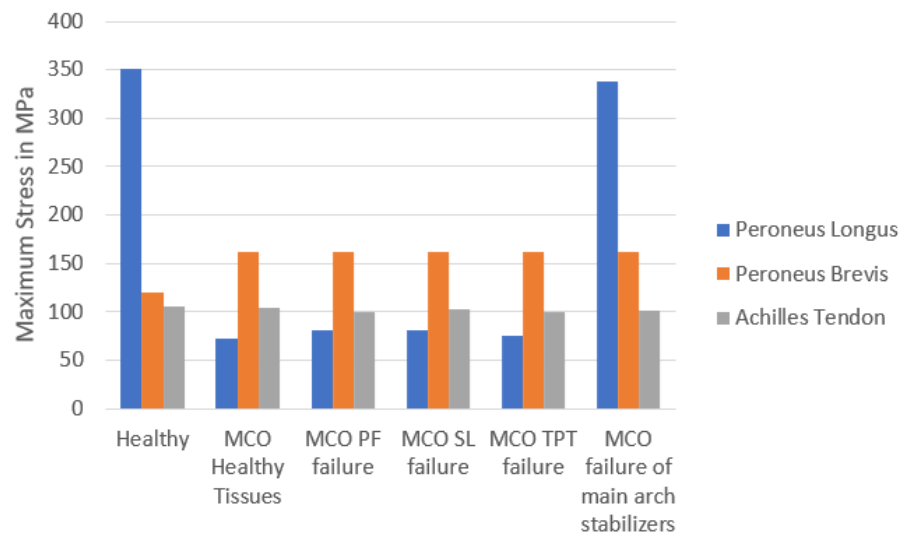


Figure 9. Comparison of the maximum stress obtained in the rest of the tendons included in the model.

4. Discussion

There are many treatment options for AAFD used by surgeons depending on the disease stage. For cases with a flexible deformity (IIa–IIb), tendon reinforcements are insufficient, requiring intervention in the bone structure. One of the most widely used options is medializing calcaneal osteotomy (MCO). Recently, Zanolli et al. and Patrick et al. [15,29] published experimental studies focused on comparing the foot's structural correction achieved with MCO with some other strategies such as Z-osteotomy or lateral column lengthening. Other authors have evaluated the outcomes of MCO and both its effect on the Achilles tendon and its contribution to correcting signs of AAFD [11]. Although the structural correction of the foot that can be achieved with MCO is widely known, some clinical studies have shown that MCO generates some long-term consequences such as stress distribution changes in the forefoot and probable risk of stress fractures, as has been reported with Evans' osteotomy [11,12,14]. These findings may be very relevant for the surgeon's decision-making process [30]. However, the biomechanical side-effects generated by MCO in both foot bones and the main soft tissues that support the plantar arch have not been analyzed sufficiently, mainly because of the difficulty of measuring tissue stress in cadaveric models [5,9].

Traditionally, the performance of an isolated arthrodesis of the cuneometatarsal joint for the treatment of flat feet in adults has been associated with a high rate of malunion. This fact has displaced the technique towards more aggressive ones, such as triple arthrodesis. However, associating an OCM reduces the pronator moment during gait and thus potentially allows it to act only on the cuneometatarsal joint. Selective arthrodesis of this joint would result in a clear clinical benefit.

In view of the above, a computational foot model was used to evaluate the changes on the biomechanics in foot tissue stresses when performing an MCO. This research alternative is used nowadays in clinical biomechanics studies. Thus, some examples such as these can be found in the literature. Smith et al. [31] designed a computational model to evaluate the structural effect of the Evans osteotomy. Wang et al. [13] proposed an FE study to evaluate different variables in MCO application, such as the angle and the medializing displacement distance. Normally, all these studies simplify the anatomy of the soft tissues and the biomechanical properties of bones. These simplifications penalize their use for analyzing the stress changes generated by MCO.

The proposed model can be reproduced, on the one hand, for loaded foot deformities and, on the other hand, for the main signs of AAFD such as foot pronation and the "too many toes" sign [4] (please see Figure 4 (bottom)). It is important to remark on two items: this model differentiates trabecular bone and cortical bone and this model contains the main soft tissues related to AAFD development. These make it possible to localize stress concentrations and evaluate stresses on both hard and soft tissues [3].

The results show that MCO effectively reduces the pronation of the hindfoot typically observed in patients with AAFD (see intense blue color around both astragalus and navicular bones). As can be seen in Figure 5, in most of the cases simulated with MCO, foot pronation was not generated. Moreover, these results indicate a good compensation of the MCO when the spring ligament fails. This is due to the supination momentum caused by the MCO over the foot structure. Nevertheless, if all the main soft tissues support the plantar arch failure, the MCO by itself cannot stop foot pronation. This means that, when performing an MCO, surgeons should add another strategy, such as arthrodeses or tendon reinforcement, for example.

Additionally, the results suggest that MCO compensates very well for the spring ligament failure. The supination momentum that MCO causes in the foot structure can explain these results. However, it is noticeable that, when all the main soft tissues that support the plantar arch fail, MCO cannot prevent foot pronation on its own. This means that MCO should be applied in combination with other strategies, such as tendon reinforcement or arthrodeses.

The results of the stress analysis on forefoot bones show that MCO reduces the bone stresses by approximately 35%, considering the healthy case as a reference and comparing the maximum stress values obtained from both healthy cases (without tissue weakness) before and after MCO (see Table 3 and Figure 6). However, when the foot arch stabilizers fail, our simulations found a stress increase in all the metatarsals, mainly in the first, second, and fourth. This increase is much more important if the plantar fascia or the tibialis posterior tendon fail, increasing the stress by approximately 34% and 28% respectively, compared to the maximum stress values obtained from MCO with healthy soft tissues (see Table 3). When the main arch stabilizers fail, the stress increases by 74%. This increase in the stress values and in its redistribution could explain the pain in the toes reported in patients treated with MCO [30] and the findings of Iaquinto [12], who concluded that corrective osteotomies shifted loads from the medial forefoot to the lateral forefoot, with greater impact for combination lateral column lengthening and MCO procedures. The stress on the third and fifth metatarsals increases less than the others, probably because of some differences in the tissue insertion on the phalanges. Despite these differences, it is important to note how the metatarsal stresses change in different scenarios.

The results of the soft tissue analysis show that MCO noticeably reduces the stress in the main foot arch stabilizers, especially when the plantar fascia (mainly) or tibialis posterior tendons fail (Figure 8). Additionally, the stress reduction generated in the peroneus longus tendon is considerable, except in the case simulated with failure of all the main foot arch stabilizers (Figure 9). This result is consistent with the structural analysis, which shows that MCO cannot correct foot pronation when these tissues fail. As expected, no significant stress changes were found in the Achilles' tendon. These results are close to those obtained by Hadfield et al. [11] and Kongsgaard et al. [32] in their study performed using cadaver models.

Finally, if some of the stabilizers of the main arch fail, such as the plantar fascia or tibialis posterior tendon, an important stress concentration around the osteotomy region appears (Table 3 and Figure 7). As is shown in Table 3, the maximum stress in these cases increased by 32% and 40%, respectively. When the foot arch stabilizers fail, the maximum stress concentration increases by about 95% (from 507 to 990 MPa). In this work, fixation methods were not evaluated since complete bone healing is assumed after calcaneal translation.

A limitation of this study is that the analysis was based on a static simulation. Thus, patients' variability in tissues and loading was not considered, because one case study was simulated. However, the relations and differences (in percentages) obtained could be useful for evaluating the MCO effects in all the scenarios simulated. Our results cannot be generalized because only one anatomy was investigated, but the relative differences obtained could help with the study of MCO effects on the foot structure. Additionally, our model does not include the plantar pad, the flexor hallucis longus, or flexor digitorum longus tendons. However, clinical studies have shown that these tissues have a minor role in AAFD development and in the foot arch support, compared to the tissues included in the model used [27,33]. Additionally, our model does not include any artificial restriction for the tibialis posterior tendon motion, so the pathway generated after traction forces may not be anatomically correct. Additionally, we used an isotropic characterization for plantar fascia and ligament tissues, which could lead to non-real calculations of stress in the tissues. It is necessary to perform a parametric study to show how sensitive the model predictions are to the material properties chosen. Moreover, our study was based on small displacements and deformations, so a linear elastic behavior for these tissues does not greatly falsify the results. This model also does not allow for error predictions, since statistics or deviations on the model characteristics are not included. One way to be able to make error predictions could be using probabilistic finite elements. Finally, it is important to remark that the values of biomechanical stress found cannot be assumed to be true stress values for all people (because of inter-subject variability). Nevertheless, we can analyze

the relative differences generated in each case. The smaller increase in the third and fifth metatarsal stresses could be caused by differences in tissue insertion in the phalanges.

5. Conclusions

As a conclusion, we can say that an MCO is a good option to perform in patients suffering with AAFD developed mainly due to a failure of the spring ligament. Nevertheless, if patients exhibit plantar fascia weakness and/or tibialis posterior tendon dysfunction, this technique could also be applied, but carefully. In this case, we found that an MCO causes an important increase in the lateral metatarsals (a possible reason for pain in the long term) and around the osteotomized area. These factors create a risk of calcaneal fracture.

Author Contributions: Conceptualization, J.B. and R.L.-G.; methodology, C.C.-D.I.P. and J.B.; software, B.D.S. and C.C.-D.I.P.; validation, C.C.-D.I.P. and R.L.-G.; formal analysis, B.D.S. and J.B.; investigation, C.C.-D.I.P. and J.B.; resources, B.D.S. and C.C.-D.I.P.; data curation, R.L.-G.; writing—original draft preparation, C.C.-D.I.P. and J.B.; writing—review and editing, J.B. and R.L.-G.; visualization, B.D.S.; supervision, C.C.-D.I.P.; project administration, J.B.; funding acquisition, J.B. All authors have read and agreed to the published version of the manuscript.

Funding: This research was funded by the Ministry of Economy and competitiveness of the Government of Spain through the project DPI2019-108009RB-100.

Data Availability Statement: All the data and results are included within the manuscript.

Conflicts of Interest: The authors declare no conflict of interest.

References

1. Abousayed, M.M.; Alley, M.C.; Shakked, R.; Rosenbaum, A.J. Adult-Acquired Flatfoot Deformity: Ethology, Diagnosis, and Management. *JBJS Rev.* **2017**, *5*, e7. [[CrossRef](#)] [[PubMed](#)]
2. Bluman, E.M.; Title, C.I.; Myerson, M.S. Posterior Tibial Tendon Rupture: A Refined Classification System. *Foot Ankle Clin.* **2007**, *12*, 233–249. [[CrossRef](#)] [[PubMed](#)]
3. Cifuentes-De la Portilla, C.; Larrainzar-Garijo, R.; Bayod, J. Biomechanical stress analysis of the main soft tissues associated with the development of adult acquired flatfoot deformity. *Clin. Biomech.* **2018**, *61*, 163–171. [[CrossRef](#)] [[PubMed](#)]
4. Deland, J.T. The adult acquired flatfoot and spring ligament complex: Pathology and implications for treatment. *Foot Ankle Clin.* **2001**, *6*, 129–135. [[CrossRef](#)] [[PubMed](#)]
5. Tao, K.; Ji, W.T.; Wang, D.M.; Wang, C.T.; Wang, X. Relative contributions of plantar fascia and ligaments on the arch static stability: A finite element study. *Biomed. Technol. Biomed. Eng.* **2010**, *55*, 265–271. [[CrossRef](#)] [[PubMed](#)]
6. Toullec, E. Adult flatfoot. *Orthop. Traumatol. Surg. Res.* **2015**, *101*, S11–S17. [[CrossRef](#)]
7. Fowble, V.A.; Sands, A.K. Treatment of adult acquired pes plano abductovalgus (flatfoot deformity): Procedures that preserve complex hindfoot motion. *Oper. Tech. Orthop.* **2004**, *14*, 13–20. [[CrossRef](#)]
8. Feibel, J.B.; Donley, B.G. Calcaneal Osteotomy and Flexor Digitorum Longus Transfer for Stage II Posterior Tibial Tendon Insufficiency. *Oper. Technol. Orthop.* **2006**, *16*, 53–59. [[CrossRef](#)]
9. Larrainzar-Garijo, R.; Cifuentes de la Portilla, C.; Gutiérrez-Narvate, E.; Díez-Nicolás, E.; Bayod, J. Efecto de la osteotomía medializante de calcáneo sobre tejidos blandos de soporte del arco plantar: Un estudio computacional. *Rev. Esp. Cir. Ortop. Traumatol.* **2018**, *63*, 15–163. [[CrossRef](#)]
10. Vora, A.M.; Tien, T.R.; Parks, B.G.; Schon, L.C. Correction of moderate and severe acquired flexible flatfoot with medializing calcaneal osteotomy and flexor digitorum longus transfer. *JBJS* **2006**, *88*, 1726–1734. [[CrossRef](#)]
11. Hadfield, M.H.; Snyder, J.W.; Liacouras, P.C.; Owen, J.R.; Wayne, J.S.; Adelaar, R.S. Effects of medializing calcaneal osteotomy on Achilles tendon lengthening and plantar foot pressures. *Foot Ankle Int.* **2003**, *24*, 523–529. [[CrossRef](#)] [[PubMed](#)]
12. Iaquinto, J.M.; Wayne, J.S. Effects of surgical correction for the treatment of adult acquired flatfoot deformity: A computational investigation. *J. Orthop. Res.* **2011**, *29*, 1047–1054. [[CrossRef](#)] [[PubMed](#)]
13. Wang, Z.; Kido, M.; Imai, K.; Ikoma, K.; Hirai, S. Towards patient-specific medializing calcaneal osteotomy for adult flatfoot: A finite element study. *Comput. Methods Biomech. Biomed. Eng.* **2018**, *21*, 332–343. [[CrossRef](#)]
14. Davitt, J.S.; Morgan, J.M. Stress fracture of the fifth metatarsal after Evans' calcaneal osteotomy: A report of two cases. *Foot Ankle Int.* **1998**, *19*, 710–712. [[CrossRef](#)]
15. Patrick, N.; Lewis, G.S.; Roush, E.P.; Kunselman, A.R.; Cain, J.D. Effects of Medial Displacement Calcaneal Osteotomy and Calcaneal Z Osteotomy on Subtalar Joint Pressures: A Cadaveric Flatfoot Model. *J. Foot Ankle Surg.* **2016**, *55*, 1175–1179. [[CrossRef](#)]
16. Tao, K.; Wang, D.; Wang, C.; Wang, X.; Liu, A.; Nester, C.J.; Howard, D. An in vivo experimental validation of a computational model of human foot. *J. Bionic Eng.* **2009**, *6*, 387–397. [[CrossRef](#)]

17. Burkhart, T.A.; Andrews, D.M.; Dunning, C.E. Finite element modeling mesh quality, energy balance and validation methods: A review with recommendations associated with the modeling of bone tissue. *J. Biomech.* **2013**, *46*, 1477–1488. [[CrossRef](#)] [[PubMed](#)]
18. Viceconti, M.; Olsen, S.; Nolte, L.-P.; Burton, K. Extracting clinically relevant data from finite element simulations. *Clin. Biomech.* **2005**, *20*, 451–454. [[CrossRef](#)]
19. Wang, Y.; Wong, D.W.-C.; Zhang, M. Computational models of the foot and ankle for pathomechanics and clinical applications: A review. *Ann. Biomed. Eng.* **2016**, *44*, 213–221. [[CrossRef](#)]
20. García-Aznar, J.M.; Bayod, J.; Rosas, A.; Larrainzar, R.; García-Bógalo, R.; Doblaré, M.; Llanos, L.F. Load transfer mechanism for different metatarsal geometries: A finite element study. *J. Biomech. Eng.* **2009**, *131*, 021011. [[CrossRef](#)]
21. Cifuentes-De la Portilla, C.; Larrainzar-Garijo, R.; Bayod, J. Analysis of the main passive soft tissues associated with adult acquired flatfoot deformity development: A computational modeling approach. *J. Biomech.* **2019**, *84*, 183–190. [[CrossRef](#)]
22. Chan, J.Y.; Williams, B.R.; Nair, P.; Young, E.; Sofka, C.; Deland, J.T.; Ellis, S.J. The contribution of medializing calcaneal osteotomy on hindfoot alignment in the reconstruction of the stage II adult acquired flatfoot deformity. *Foot Ankle Int.* **2013**, *34*, 159–166. [[CrossRef](#)]
23. Wright, D.G.; Rennels, D.C. A Study of the Elastic Properties of Plantar Fascia. *JBJS* **1964**, *46*, 482–492. [[CrossRef](#)]
24. Morales-Orcajo, E.; Souza, T.R.; Bayod, J.; de Las Casas, E.B. Non-linear finite element model to assess the effect of tendon forces on the foot-ankle complex. *Med. Eng. Phys.* **2017**, *49*, 71–78. [[CrossRef](#)] [[PubMed](#)]
25. Wu, L. Nonlinear finite element analysis for musculoskeletal biomechanics of medial and lateral plantar longitudinal arch of Virtual Chinese Human after plantar ligamentous structure failures. *Clin. Biomech.* **2007**, *22*, 221–229. [[CrossRef](#)] [[PubMed](#)]
26. Bayod, J.; Becerro-de-Bengoa-Vallejo, R.; Losa-Iglesias, M.E.; Doblaré, M. Mechanical stress redistribution in the calcaneus after autologous bone harvesting. *J. Biomech.* **2012**, *45*, 1219–1226. [[CrossRef](#)]
27. Arangio, G.A.; Salathe, E.P. A biomechanical analysis of posterior tibial tendon dysfunction, medial displacement calcaneal osteotomy and flexor digitorum longus transfer in adult acquired flat foot. *Clin. Biomech.* **2009**, *24*, 385–390. [[CrossRef](#)]
28. Gefen, A. Stress analysis of the standing foot following surgical plantar fascia release. *J. Biomech.* **2002**, *35*, 629–637. [[CrossRef](#)] [[PubMed](#)]
29. Zanolli, D.H.; Glisson, R.R.; Nunley, J.A.; Easley, M.E. Biomechanical assessment of flexible flatfoot correction: Comparison of techniques in a cadaver model. *JBJS* **2014**, *96*, 45. [[CrossRef](#)]
30. Guha, A.R.; Perera, A.M. Calcaneal osteotomy in the treatment of adult acquired flatfoot deformity. *Foot Ankle Clin.* **2012**, *17*, 247–258. [[CrossRef](#)]
31. Smith, B.A.; Adelaar, R.S.; Wayne, J.S. Patient specific computational models to optimize surgical correction for flatfoot deformity. *J. Orthop. Res.* **2016**, *35*, 1523–1531. [[CrossRef](#)] [[PubMed](#)]
32. Kongsgaard, M.; Aagaard, P.; Kjaer, M.; Magnusson, S.P. Structural Achilles tendon properties in athletes subjected to different exercise modes and in Achilles tendon rupture patients. *J. Appl. Physiol.* **2005**, *99*, 1965–1971. [[CrossRef](#)] [[PubMed](#)]
33. Riddiford-Harland, D.; Steele, J.; Baur, L. Medial midfoot fat pad thickness and plantar pressures: Are these related in children? *Int. J. Paediatr. Obes.* **2011**, *6*, 261–266. [[CrossRef](#)] [[PubMed](#)]

Disclaimer/Publisher’s Note: The statements, opinions and data contained in all publications are solely those of the individual author(s) and contributor(s) and not of MDPI and/or the editor(s). MDPI and/or the editor(s) disclaim responsibility for any injury to people or property resulting from any ideas, methods, instructions or products referred to in the content.